

Coherent detection of orbital angular momentum in radio

L. K. S. Daldorff, The Catholic University of America, Washington, DC, USA
S. M. Mohammadi, Infotrek, Stockholm, Sweden
J. E. S. Bergman, Swedish Institute of Space Physics, Uppsala, Sweden
B. Isham, Interamerican University of Puerto Rico, Bayamón, Puerto Rico, USA
M. K. T. Al-Nuaimi, Southeast University, Nanjing, China
K. Forozesh, Upplysningscentralen AB, Stockholm, Sweden
T. D. Carozzi, Chalmers University of Technology, Gothenburg, Sweden

Abstract: The angular momentum propagated by a beam of radiation has two contributions: spin angular momentum (SAM) and orbital angular momentum (OAM). SAM corresponds to wave polarisation, while OAM-carrying beams are characterized by a phase which is a function of azimuth. We demonstrate experimentally that radio beams propagating OAM can be generated and coherently detected using ordinary electric dipole antennas. The results presented here could pave the way for novel radio OAM applications in technology and science, including radio communication, passive remote sensing, and new types of active (continuous or pulsed transmission) electromagnetic measurements.

Manuscript date: 23 December 2015

As early as 1909 the wave motions associated with a revolving shaft were studied by Poynting, who suggested, by analogy, that circularly-polarised light should carry angular momentum (OAM) (Poynting, 1909). In 1936 Beth reported on an optical experiment (Beth, 1936) in which he verified Poynting's prediction. Since then others have studied electromagnetic OAM (Carrara, 1949; di Francia, 1957; Allen, 1966), however it is only recently that electromagnetic OAM has been extensively studied and utilized, both theoretically (Mair et al., 2001; Thidé et al., 2007; Mohammadi et al., 2010b,a; Thidé et al., 2011; Bennis et al., 2013) and experimentally, at visible (Allen et al., 1992; Beijersbergen et al., 1994; Paterson, 2005; Lavery et al., 2013a,b), millimeter and microwave (Hajnal, 1990; Kristensen et al., 1994; Turnbull et al., 1996; Courtial et al., 1998; Jiang et al., 2009; Cheng et al., 2014), and radio wavelengths (Leyser et al., 2009; Tamburini et al., 2012). OAM has also been studied in electron beams (McMorran et al., 2011). In addition to energy and linear momentum, electromagnetic waves can propagate angular momentum to infinity. The total electromagnetic angular momentum

has mode numbers $j = s + l$, where s and l are mode numbers, respectively, of the electromagnetic spin and orbital angular momentum (Humblet, 1943). Classically, spin angular momentum manifests itself as wave polarisation, where mode numbers $s = \pm 1$ correspond to right- and left-hand circularly polarised modes and $s = 0$ to linearly-polarised modes. Similarly, OAM-carrying beams are characterized by a phase which is a function of azimuth, and OAM mode numbers l are classically manifested by a change in phase of $l \times 360^\circ$ around any arbitrary circle centred on the beam axis (Allen *et al.*, 1992; Turnbull *et al.*, 1996).

We extend the radio angular momentum technique (Carrara, 1949; Allen, 1966; Hajnal, 1990; Kristensen *et al.*, 1994; Courtial *et al.*, 1998; Jiang *et al.*, 2009; Liska and Meinke, 1970; Leysner *et al.*, 2009; Mohammadi *et al.*, 2010b,a; Thidé *et al.*, 2007, 2011) by actively generating OAM radio beams having a variety of mode numbers using a simple antenna array (Thidé *et al.*, 2007), and by using a phase-coherent technique to detect and verify the transmitted modes (Mohammadi *et al.*, 2010a). The results presented here demonstrate that radio beams propagating OAM can be generated (Thidé *et al.*, 2007; Mohammadi *et al.*, 2010b) and coherently detected (Mohammadi *et al.*, 2010a) using ordinary electric dipole antennas. This could potentially pave the way for novel radio OAM applications in technology and science, including radio communication, radio and radar remote sensing, ionospheric radio diagnostics, and radio astronomy. Note that, using current technology, it is only at radio frequencies that coherent measurements of electromagnetic fields, *i.e.* measurement of both amplitude and phase, may be performed.

An antenna array of N identical sources at angular frequency ω and equal amplitudes has the array factor

$$\Psi = \sum_{n=1}^N \exp[-i(\vec{k} \cdot \vec{x}_n - \phi_n)], \quad (1)$$

where \vec{k} is the wave vector, \vec{x}_n is the position, ϕ_n is the phase of the n th emitter, and i represents $\sqrt{-1}$ (Mohammadi *et al.*, 2010b; Balanis, 2005; Chireix, 1936; Knudsen, 1953). When the emitters are electric dipoles with dipole moments \vec{d} , the electromagnetic energy density $u = \epsilon_0(|\vec{E}|^2 + c^2|\vec{B}|^2)/2$, where \vec{E} and \vec{B} are the electric and magnetic fields, becomes

$$u = \frac{k^2 |\vec{k} \times \vec{d}|^2 |\Psi|^2}{\epsilon_0 (4\pi r)^2} + O(r^{-3}), \quad (2)$$

where ϵ_0 is the vacuum permittivity and $r = |\vec{x}|$ is the radial distance from the centre of the array, where \vec{x} is the position vector. The total angular momentum

density is defined as $\vec{h} = \vec{x} \times \vec{g}$, where $\vec{g} = \epsilon_0 \text{Re}\{\vec{E} \times \vec{B}^*\}$ is the linear momentum density. In our case we have linearly-polarised dipoles, *i.e.* $\vec{d} \times \vec{d}^* = \vec{0}$ and $s = 0$, so that the total angular momentum $j = l + s = l$. Hence, only the OAM contributes to the total angular momentum density,

$$\vec{h} = \frac{u}{\omega} \frac{\Re\Psi^* \widehat{L}\Psi}{|\Psi|^2} + \vec{O}(r^{-3}), \quad (3)$$

where $\widehat{L} = -i(\vec{x} \times \nabla)$ is the OAM operator. Since the OAM operator in Eq. 3 only operates on the array factor Ψ , the only contribution to the angular momentum of the fields will be from the phasing of the elements and the geometry of the array, not the individual antenna elements, so long as the elements are much smaller than the size of the array.

We have used a circular array of $N = 6$ elements placed in the xy plane with emitters distributed equidistantly around the perimeter of a circle of radius a as shown in fig. 1, and phased such that $\phi_n = 2\pi ln/N$, with l an integer. The array factor becomes

$$\Psi_l = N(-i)^l \exp(il\varphi) J_l(ka \sin\theta), \quad (4)$$

where, θ and φ are the spherical polar and azimuthal angles, respectively, and J_l is the Bessel function. The array factor Ψ_l contains the phasor $\exp(il\varphi)$ which is a characteristic of OAM beams (Allen *et al.*, 1992). The phase factor varies around the beam axis and the OAM number, l , corresponds to a Fourier component. Thus, by measuring the phase of a single field component, the OAM modes can be separated by a spatial Fourier transform about the z axis (Elias II, 2008).

An array of $N = 6$ folded half-wavelength dipole antennas was constructed, as shown in the inset in fig. 1. The transmitting antennas were numerically simulated using the method-of-moments-based EM simulator Ansoft Designer SV and fabricated using LPKF prototyping PCB milling machine on RO4003C dielectric material, which has dielectric constant 3.38, dissipation factor $\tan(\delta) = 0.0027$, and copper thickness 0.018 mm (Rogers Corporation, 2015). The antennas were fed with equal amplitudes and with phase shifts of $\delta\phi = 0^\circ, \pm 60^\circ$, and $\pm 120^\circ$ between consecutive elements, such that the array generated beams carrying OAM modes $l = 0, \pm 1$, and ± 2 , respectively. The radiation patterns of the simulated beams are shown in fig. 2. In the simulations, ordinary dipoles were used instead of folded dipoles for simplicity. NEC-4 (Adler, 1993) was used for modeling the beams.

As can be seen in the phase plots in the upper panels of fig. 3, when looking up the beam towards the transmitting array (*i.e.* towards the page in fig. 3), the

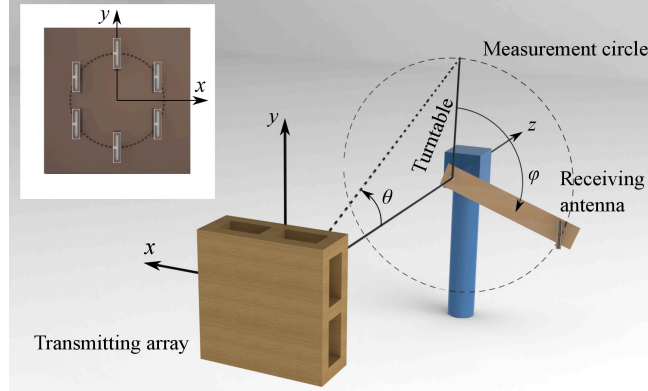


Figure 1: The experimental setup. The six-element transmitting antenna array is at the lower left, at the origin of the coordinate system, with a front view of the array shown in the inset at top left. The receiving antenna is located to the right, at the end of a rotating arm. The arm was connected to the turntable, the pivot of which was located on the z axis, and which was supported by a vertical pillar (blue) connected to the floor. The transmitting antennas were half-wavelength folded dipoles directed along the vertical, parallel to the y axis, positioned equidistantly around a circle of radius $a = 0.75\lambda$ (where λ is the wavelength) and placed parallel to, and at a distance of 0.013 m (0.1λ) in front of, a conducting plane. The xy plane, and the dashed circle of the transmitting array (see inset), were parallel to a chamber wall, and the z axis was perpendicular to the same wall. By feeding the transmitting antennas with equal amplitudes and with a phase difference between consecutive elements of 0° , $\pm 60^\circ$, and $\pm 120^\circ$, OAM modes $l = 0$, $l = \pm 1$, and $l = \pm 2$, respectively, were generated. The centre axis of the horizontally-transmitted beam was aligned with the rotation axis of the rotating arm. The receiving antenna was attached to the arm, so that it rotated around the beam axis at a radius of 1.00 meter, thus avoiding the null at the centre of the OAM beams. The measurement plane was located 4.82 m (38.3λ) from the transmitting array; the angle θ was 11.7° . During the measurements, the arm was rotated in a vertical plane, parallel to the xy plane. The receiving antenna was vertically-aligned and measured the y component of the transmitted electric field.

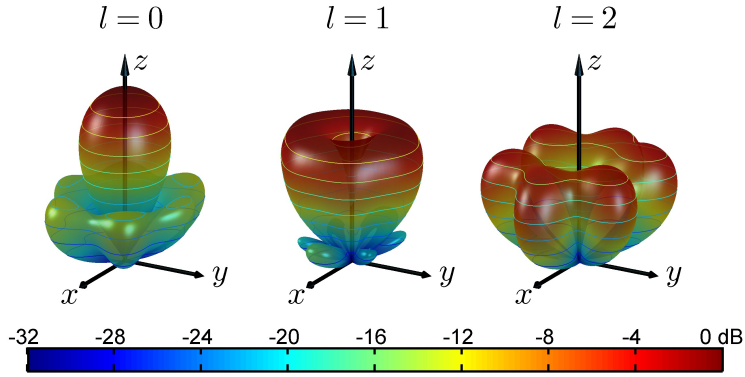


Figure 2: Simulated radiation patterns for the $l = 0, \pm 1$, and ± 2 radio beams. For $l \neq 0$ the beams exhibit the characteristic null along the beam axis ($\theta = 0^\circ$) (Thidé *et al.*, 2007; Mohammadi *et al.*, 2010b,a; Josefsson and Persson, 2006). Simulations, analytical calculations, and measurements show that the $l = 0$ and ± 1 beams have maxima at $\theta = 0^\circ$ and $\theta = 22^\circ$, respectively. For $l = \pm 2$, the angle of the beam varied significantly around the beam axis. This is because $l = \pm 2$ is much closer to the theoretical limit in the inequality $|l| < N/2$ for unambiguous transmission of OAM modes; the OAM beam will degrade as the limit is approached. Note also that the amplitude patterns for $l = \pm 2$ exhibit ripples. Small ripples were also present for $l = \pm 1$ but are not visible in the figure. Ripples generally appear when $|l|$ approaches the upper limit of $N/2$. The color scale and contour lines indicate power density for each beam relative to the maximum of the $l = 0$ beam; the interval between contour lines is 3.2 dB.

lines of constant phase spiral out from the beam axis counterclockwise for $l > 0$ (right-handed) and clockwise (left-handed) for $l < 0$. One complete turn at constant radius around the beam axis changes the phase of the field components by $l \times 360^\circ$. Accordingly, for the measurements presented here, the phase of E_y , which is the strongest electric field component, was measured at a constant radius from the beam axis (Mohammadi *et al.*, 2010a).

The measurements took place in an anechoic chamber at a frequency of 2.383 GHz (corresponding to a wavelength, λ , of 0.126 m) and at a distance of $z = 4.82$ m (38.3λ) from the transmitting array and hence well into the far-field region. The E_y field was measured with a half-wave dipole antenna made from brass bars, connected to a $\lambda/4$ bazooka balun fabricated from rigid co-axial cable, and placed at the tip of a one-meter-long rotating arm, which was mounted on a pillar attached to the floor, see fig. 1. The amplitude and phase of E_y were measured every 4° , for $l = 0, \pm 1$, and ± 2 . Repeated measurements for $l = 1$ showed that the beam amplitude and phase were stable.

For $l = 0$ the measured data show a sinusoidally-oscillating, rather than constant, phase around the measurement circle. This oscillation was found to be produced by a small misalignment between the centre of the transmitted beam and the centre of the measurement circle. This misalignment also produced a periodic phase oscillation in the $l = \pm 1$ and ± 2 data. The $l = 0$ measurement was used to correct the phase data for all modes. The ripples in the phase plots in the lower panels of fig. 3 indicate the effect of spatial reflections of the signal and that the transmission was not a pure OAM mode, as can be expected from the variation of the beam maximum around the beam axis in the radiation pattern for $l = 1$ and 2 in fig. 2.

Fig. 4 shows the measured l spectra, computed by means of a spatial Fourier transform about the z axis (see Eq. 4 above). Only minor errors arise at the transmitting side, where the feeding network delivered a maximum phase error of 3° and a maximum amplitude difference of 0.03 dB to the six transmitting antennas. These antennas were well-tuned and less than 2% of the power was reflected back to the transmitter. The spread in the spectrum is primarily due to the finite number of transmit antennas and the reflections in the measurement chamber. The spectra confirm that the intended OAM modes were transmitted and correctly detected.

In summary, we have generated several radio OAM modes using a circular antenna array and successfully verified these modes via measurements of a single electric field component using an ordinary electric half-wave dipole; the detection of OAM does not require the use of a receiving array or a measurement of the full electric and magnetic field vectors. In addition, we have demonstrated that it is sufficient to measure the phase rotation to determine the OAM mode of a

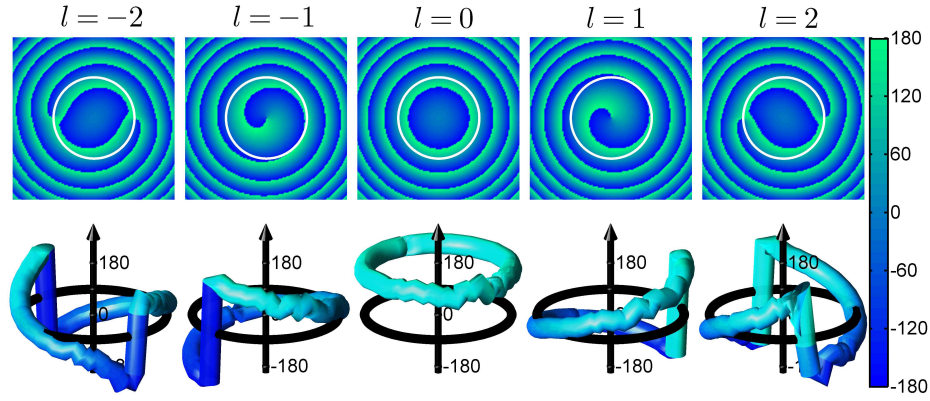


Figure 3: Simulated and measured phase distributions in the OAM beam. In the upper panels the positive z axis is out of the paper, in the lower panels the positive z axis is oriented upwards. The upper panels show the simulated OAM beam phase distribution for the y component of the electric field at the measurement plane. From left to right, the panels show the phase for $l = -2, -1, 0, 1,$ and 2 , as seen looking along the beam axis toward the transmitting array, *i.e.* in the negative z direction. The white circle indicates the position of the measurement circle. The lower panels show the measured phase of the y component of the electric field. The measured phase is indicated by both colour and vertical displacement. The OAM mode is found by counting the number of branch cuts from -180° to $+180^\circ$, *i.e.* for $|l| = 0, 1,$ and 2 we have $0, 1,$ and 2 branch cuts, respectively. The orientation of the phase slope gives the sign of the measured OAM mode. Declining phase values when the xy plane is traversed in a right-handed sense indicate a negative mode, and increasing values a positive mode. The distortions visible in the measured phase are due to increased reflection when the receiving antenna is close to the floor. The color bar at right shows phase in degrees; both the upper and lower panels use the same color scale.

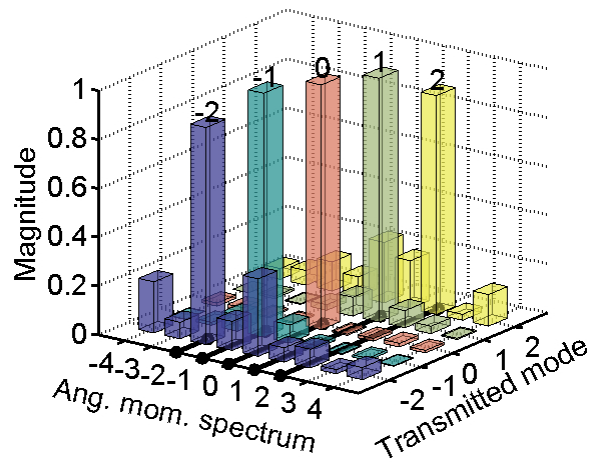


Figure 4: Angular momentum spectra. Five data sets of 90 phase measurements each were taken every 4° around the measurement circle. Each set was Fourier transformed, from φ space to l space. The magnitudes of the Fourier components corresponding to OAM mode numbers $-4 \leq l \leq 4$ are shown. The spectra show some leakage between mode numbers but the peaks are well correlated with the intended OAM modes, $-2 \leq l \leq 2$. The magnitude scale is normalized for each mode such that the sum of the magnitudes from $l = -45$ to $l = +44$ is equal to 1.

radio beam. Although the power pattern for the $|l| = 2$ beams was not ideal, the spatial phase patterns are insensitive to imperfections in the beam, and the measured phase depends only weakly on azimuthal field strength fluctuations and on the accuracy of the circular measurement path around the beam axis (*Mohammadi et al.*, 2010a,b).

This experiment opens up new possibilities for radio communications and for radio and radar remote sensing of rotational phenomena in the atmosphere and space. Backscatter from OAM-modulated radar observations of the ionosphere can be analyzed using the methods presented here to diagnose possible rotational properties of plasma processes. Artificially-induced and natural radio emissions from the ionospheric plasma (*Leyser*, 2001; *LaBelle and Treumann*, 2002; *Leyser et al.*, 2009) could be analyzed for possible OAM effects, lending clues to plasma processes. The large-array radio telescopes recently constructed and being planned could be used to search for signs of electromagnetic OAM arriving from astrophysical plasmas (*Harwit*, 2003; *Elias II*, 2008). Each OAM mode can act as an independent channel for transmission and reception, suggesting the possibility of increasing the information transfer rate within existing measurement and communications bands (*Edfors and Johansson*, 2012; *Tamburini et al.*, 2012). The information carried in OAM modes may also allow radio and radar imaging at resolutions below the Rayleigh limit (*Li and Li*, 2013). In all applications, the reception of weak radio signals located close to an undesired strong source might be improved by orienting the central null in an OAM receiving antenna towards the undesired source. For example, radio observations of the solar corona could be performed by placing the central null in an OAM beam over the radio-bright disk of the sun.

Acknowledgments: We thank Roger Karlsson, Lennart Åhlén, Walter Puccio, Sven-Erik Jansson, Farid Shiva, Thomas Oswald, Erland Cassel, Shi Cheng, and Johan Lindberg for technical support and advice. We thank Anders Rydberg and Anders Ahlén for loaning equipment and for allowing access to the new Ångström Laboratory antenna chamber, which was funded by the Knut and Alice Wallenberg Foundation. We thank the electronics lab of the Swedish Institute of Space Physics in Uppsala for granting access to their facilities, lending equipment, and for covering the electrical equipment expenses. We thank Masih Noor at the Center for Accelerator and Instrument Development for help with the CAD drawing for Figure 1 and Anders Hast and Martin Ericsson at UPPMAX for valuable help and feedback in visualizing the antenna patterns. We thank Bo Thidé for providing the inspiration for this work. The construction materials and personnel hours required for the experiment were privately financed by the authors. S. M. M.

thanks Interamerican University of Puerto Rico for its hospitality during part of this work. B. I. was supported by ARO grant W911NF-10-1-0002. We also thank the referees for constructive and helpful comments.

References

- Adler, D. (1993), Information on the history and availability of NEC-MOM codes for PCs and unix, *Applied Computational Electromagnetics Society Newsletter*, 8(3), 8–10, http://www.nec2.org/nec_hist.txt, accessed 2015-08-30.
- Allen, L., M. W. Beijersbergen, R. J. C. Spreeuw, and J. P. Woerdman (1992), Optical angular momentum of light and the transformation of Laguerre-Gauss laser modes, *Phys. Rev. A Gen. Phys.*, 45, 8185–8189.
- Allen, P. J. (1966), A radiation torque experiment, *Am. J. Phys.*, 34, 1185–1192, doi:<http://dx.doi.org/10.1119/1.1972585>.
- Balanis, C. A. (2005), *Antenna Theory*, 3 ed., John Wiley and Sons, New York.
- Beijersbergen, M. W., R. P. C. Coerwinkel, M. Kristensen, and J. P. Woerdman (1994), Helical-wavefront laser beams produced with a spiral phaseplate, *Optics Comm.*, 112, 321–327, doi:[http://dx.doi.org/10.1016/0030-4018\(94\)90638-6](http://dx.doi.org/10.1016/0030-4018(94)90638-6).
- Bennis, A., R. Niemiec, C. Brousseau, K. Mahdjoubi, and O. Emile (2013), Flat plate for oam generation in the millimeter band, in *7th European Conference on Antennas and Propagation (EuCAP)*, art. no. 6546903.
- Beth, R. A. (1936), Mechanical detection and measurement of the angular momentum of light, *Phys. Rev.*, 50(2), 115–125.
- Carrara, N. (1949), Torque and angular momentum of centimetre electromagnetic waves, *Nature*, 164, 882–884, doi:<http://dx.doi.org/10.1038/164882c0>.
- Cheng, L., W. Hong, and Z.-C. Hao (2014), Generation of electromagnetic waves with arbitrary orbital angular momentum modes, *Sci. Rep.*, 4(1484), 5 pp., doi:<http://dx.doi.org/10.1038/srep04814>.
- Chireix, H. (1936), Antennas á rayonnement zénital réduit, *L'Onde Élec.*, 15, 440–456.

- Courtial, J., K. Dholakia, D. A. Robertson, L. Allen, and M. J. Padgett (1998), Measurement of the rotational frequency shift imparted to a rotating light beam possessing orbital angular momentum, *Phys. Rev. Lett.*, *80*, 3217–3219, doi: <http://dx.doi.org/10.1103/PhysRevLett.80.3217>.
- di Francia, G. T. (1957), On a macroscopic measurement of the spin of electromagnetic radiation, *Nuov. Cim.*, *6*, 150–167.
- Edfors, O., and A. J. Johansson (2012), Is orbital angular momentum (OAM)-based radio communication an unexploited area?, *IEEE Transactions on Antennas and Propagation*, *60*, 1126–1131, doi:<http://dx.doi.org/10.1109/TAP.2011.2173142>.
- Elias II, N. M. (2008), Photon orbital angular momentum in astronomy, *Astron. Astrophys.*, *492*(3), 883–922, doi:<http://dx.doi.org/10.1051/0004-6361:200809791>.
- Hajnal, J. V. (1990), Observations of singularities in the electric and magnetic fields of freely propagating microwaves, *Proc. Roy. Soc. London A*, *430*, 413–421, doi:<http://dx.doi.org/10.1098/rspa.1990.0097>.
- Harwit, M. (2003), Photon orbital angular momentum in astrophysics, *Astrophys. J.*, *597*, 1266–1270, doi:<http://dx.doi.org/10.1086/378623>.
- Humblet, J. (1943), Sur le moment d’impulsion d’une onde électromagnétique, *Physica*, *X*(7), 585–603.
- Jiang, Y., Y. He, and F. Li (2009), Wireless communications using millimeter-wave beams carrying orbital angular momentum, in *Conference on Communications and Mobile Computing*, vol. 1, pp. 495–500, Kunming, Yunnan, China.
- Josefsson, L., and P. Persson (2006), *Conformal Array Antenna Theory and Design*, Wiley-Interscience.
- Knudsen, H. L. (1953), The field radiated by a ring quasi-array of an infinite number of tangential or radial dipoles, *Proc. IRE*, *41*, 781–789.
- Kristensen, M., M. W. Beijersbergen, and J. P. Woerdman (1994), Angular momentum and spin-orbit coupling for microwave photons, *Optics Comm.*, *104*, 229–233, doi:[http://dx.doi.org/10.1016/0030-4018\(94\)90547-9](http://dx.doi.org/10.1016/0030-4018(94)90547-9).

- LaBelle, J., and R. A. Treumann (2002), Auroral radio emissions, 1: Hisses, roars, and bursts, *Space Sci. Rev.*, *101*(3), 295–440.
- Lavery, M. P. J., D. J. Robertson, A. Sponselli, J. Courtial, N. K. Steinhoff, G. A. Tyler, A. E. Willner, and M. J. Padgett (2013a), Efficient measurement of an optical orbital-angular-momentum spectrum comprising more than 50 states, *New Journal of Physics*, *15*(1), 013024, doi:<http://dx.doi.org/10.1088/1367-2630/15/1/013024>.
- Lavery, M. P. J., F. C. Speirits, S. M. Barnett, and M. J. Padgett (2013b), Detection of a spinning object using light's orbital angular momentum, *Science*, *341*, 537–540, doi:10.1126/science.1239936.
- Leyser, T. B. (2001), Stimulated electromagnetic emissions by high-frequency electromagnetic pumping of the ionospheric plasma, *Space Sci. Rev.*, *98*, 223–328.
- Leyser, T. B., L. Norin, M. McCarrick, T. R. Pedersen, and B. Gustavsson (2009), Radio pumping of ionospheric plasma with orbital angular momentum, *Phys. Rev. Lett.*, *102*(6), 065004, doi:<http://dx.doi.org/10.1103/PhysRevLett.102.065004>.
- Li, L., and F. Li (2013), Beating the Rayleigh limit: Orbital-angular-momentum-based super-resolution diffraction tomography, *Phys. Rev. E*, *88*, 033,205, doi:<http://dx.doi.org/10.1103/PhysRevE.88.033205>.
- Liska, H., and H. Meinke (1970), Der experimentelle Nachweis der beiden elementaren Typen von Energiewirbeln in Wellenfeldern, *Nachrichtentechnische Zeit.*, *23*, 445–448.
- Mair, A., A. Vaziri, G. Weihs, and A. Zeilinger (2001), Entanglement of the orbital angular momentum states of photons, *Nature*, *412*, 313–316, doi:<http://dx.doi.org/10.1038/35085529>.
- McMorran, B. J., A. Agrawal, I. M. Anderson, A. A. Herzing, H. J. Lezec, J. J. McClelland, and J. Unguris (2011), Electron vortex beams with high quanta of orbital angular momentum, *Science*, *331*, 192–195, doi:<http://dx.doi.org/10.1126/science.1198804>.
- Mohammadi, S. M., L. K. S. Daldorf, K. Forozesh, B. Thidé, J. E. S. Bergman, B. Isham, R. Karlsson, and T. D. Carozzi (2010a), Orbital angular momentum

- in radio: Measurement methods, *Radio Sci.*, 45, RS4007–1–RS4007–14, doi:
<http://dx.doi.org/10.1029/2009RS004299>.
- Mohammadi, S. M., L. K. S. Daldorff, J. E. S. Bergman, R. L. Karlsson, B. Thidé,
K. Forozesh, T. D. Carozzi, and B. Isham (2010b), Orbital angular momentum
in radio: A system study, *IEEE Trans. Antennas Propagat.*, 58, 565–572.
- Paterson, C. (2005), Atmospheric turbulence and orbital angular momentum of
single photons for optical communication, *Phys. Rev. Lett.*, 94(15), 153,901.
- Poynting, J. H. (1909), The wave motion of a revolving shaft, and a suggestion as
to the angular momentum in a beam of circularly polarised light, *Proc. Royal
Society London*, A82, 560–567, doi:<http://dx.doi.org/10.1098/rspa.1909.0060>.
- Rogers Corporation (2015), RO4000 series high frequency circuit materials, *Tech.
rep.*, publication no. 92-004, url: [https://www.rogerscorp.com/documents/726/
acm/RO4000-Laminates—Data-sheet.pdf](https://www.rogerscorp.com/documents/726/acm/RO4000-Laminates—Data-sheet.pdf).
- Tamburini, F., E. Mari, A. Sponselli, B. Thidé, A. Bianchini, and F. Romanato
(2012), Encoding many channels on the same frequency through radio vorticity:
first experimental test, *New Journal of Physics*, 14(3), 033,001, doi:[http://dx.
doi.org/10.1088/1367-2630/14/3/033001](http://dx.doi.org/10.1088/1367-2630/14/3/033001).
- Thidé, B., H. Then, J. Sjöholm, K. Palmer, J. E. S. Bergman, T. D. Carozzi, Y. N.
Istomin, N. H. Ibragimov, and R. Khamitova (2007), Utilization of photon
orbital angular momentum in the low-frequency radio domain, *Phys. Rev. Lett.*,
99(8), 087,701.
- Thidé, B., J. Lindberg, H. Then, and F. Tamburini (2011), Linear and angular
momentum of electromagnetic fields generated by an arbitrary distribution of
charge and current densities at rest, *ArXiv e-prints*, p. 5 p.
- Turnbull, G. A., D. A. Robertson, G. M. Smith, L. Allen, and M. J. Padgett (1996),
The generation of free-space Laguerre-Gaussian modes at millimetre-wave fre-
quencies by use of a spiral phaseplate, *Optics Comm.*, 127, 183–188.